DIAGNOSTYKA, 2017, Vol. 18, No. 4

ISSN 1641-6414
e-ISSN 2449-5220

DIAGNOSING OF FATIGUE LIFESPAN USING THE MODERN METHOD OF WELDING SIMULATING

Miroslav BLATNICKY, Dalibor BARTA, Jan DIZO[1], Pawel DROZDZIEL[2]

[1] University of Zilina, Faculty of Mechanical Engineering, Univerzitná 1, 010 26 Zilina, Slovakia, e-mail: miroslav.blatnicky@fstroj.uniza.sk
[2] Lublin University of Technology, Mechanical Engineering Faculty, Nadbystrzycka 38 D, 20 – 618 Lublin, Poland, e-mail: p.drozdziel@pollub.pl

Abstract

The paper deals with analytical determination of the stress concentrator location on a sample serving for diagnosing multiaxial fatigue lifespan of aluminium alloys, which are applied for reducing weight of road and rail vehicle constructions for acquiring decrease of fuel consumption. This article put emphasis on significance of appropriate sample design and notch location according to the material type and mounting in the testing device. It operates also with suitable welding technology selection and thus ensures input parameters for numerical simulations of selected welding technology. The aim of numerical simulations is obtaining important information that will serve for detailed fatigue lifespan prediction in comparison of base and weld material.

Keywords: fatigue, aluminium alloy, welding, simulation

DIAGNOZOWANIE WYTRZYMAŁOŚCI ZMĘCZENIOWEJ PRZY UŻYCIU NOWOCZESNEJ METODY SYMULACJI SPAWANIA

Artykuł dotyczy analitycznego wyznaczania położenia koncentratora naprężeń w próbce służącej do diagnozowania wieloosiowej wytrzymałości stopów aluminium stosowanych do zmniejszenia wagi konstrukcji pojazdów drogowych i kolejowych w celu mniejszego zużycia paliwa. W artykule położono nacisk na znaczenie odpowiednich wymagań technicznych próbki, a także położenia wycięcia w zależności od typu materiału i mocowania w urządzeniu do testowania. Poruszono również kwestię wyboru odpowiedniej technologii spawania, dzięki czemu parametry wejściowe dla numerycznych symulacji wybranej technologii spawania są dobierane we właściwy sposób. Celem symulacji numerycznych jest uzyskanie ważnych informacji, które posłużą do przewidywania szczegółowej wytrzymałości zmęczeniowej w odniesieniu do materiału rodzimego i złącza spawanego

Słowa kluczowe: zmęczenie (materiału), stop aluminium, spawanie, symulacja

1. INTRODUCTION

The usage of materials is limited by their properties. Material is in general a substance intended for further processing. All materials and not only they are subjected to ageing, fatigue or wear [1]. This is the reason for the effort to decrease the effect of such adverse conditions, and thus increase the resistance of the material over the longest period of operation as possible, which is actually the reason for saving in material costs. Further, there is a tendency to produce equipment with more power at reduced weight in conjunction with the speed growth of the individual parts of mechanisms. There may be operating temperatures- or the load-increase and possibly other operating parameters. Components made from new types of materials are able to withstand all these conditions thanks to new technologies of production, heat treatment and as in practice comes to the integration of components into larger groups as well as through new technologies in welding. Unfortunately, not even component made from the "best material" can perform its function forever. After some time there is degradation of all its characteristics. One of the most common manifestations of the component operation is fatigue. Fatigue is also a one of the most dangerous processes causing material damage because it can cause harm to the components that worked many hours of operation without any sign of wear. This is due to the gradual violation of material cohesion by time dependent state of stress as a result of the accumulation of damage by alternating elastic - plastic deformation (already at the micro-level) [2, 3]. Whereas, in technical practice it is not only the use of simple one-piece components but they are able to join into larger structural units by the different technologies, also these connections are subjected to physical laws, wear and fatigue, hence the degradation takes place.

One of technologies of permanent fixed connection of materials is welding. Depending on the type of base material the weld material has equal or higher strength than base material.

2. TESTED BASE MATERIAL

As an experimental material to perform multiaxial fatigue test the commercial aluminium alloy EN AW 6063.T66 (AlMgSi07.F25) with a standard chemical composition was selected (Table. 1). This material was used because of the increased use of aluminium alloys, especially in the developed automotive industry, because there is a trend to replace ferrous materials by non-ferrous metals and aluminium is on the top in the use of the other non-ferrous metals.

Si	0,2 - 0,6 %
Fe	0,35 %
Cu	0,1 %
Mn	0,1 %
Mg	0,45 - 0,9 %
Cr	0,1 %
Ni	-
Zn	0,1 %
Ti	0,1 %
other elements	max. 0,05 % each max. 0,15 % total
Al	remaining %

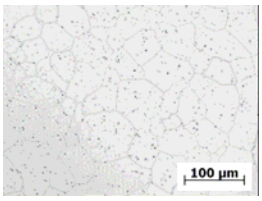

Fig. 1. Standardised chemical composition of the tested material (above) and its microstructure in the longitudinal direction (down) 0.5% HF etched

AlMgSi0.7 microstructure in the longitudinal direction observed by light microscope is shown in Fig. 1. According to the figure it can be concluded that the structure is composed of polyhedral grain roughly the same size. In grains of the base material can be observed uniformly distributed intermetallic phases and at the grain boundaries have been detected segregates.

3. SAMPLE GEOMETRY

There is a requirement of the structural notch creation to act as a stress-raiser prior to experimental samples measurement, which means formation of a place where crack initiation and its growth until sample failure can be expected [4]. The notch shape as seen in the Fig. 2 was chosen in view of its relatively undemanding creation on the sample and also because there are measurements of fatigue of materials with similarly shaped stress-raisers. The sample will be stored in the jaws of diagnostic equipment where will be multiaxially stressed [5] in suitable manner until the sample failure. The sample gripping explains Fig. 2.

Fig. 2. Stress diagnostic system for cyclic bending and torsion stress of testing samples

The jaw in the Fig. 2 left causes the bending stress of the sample and the right jaw causes torsion stress. Since the drives of the tester are independent of each other, it is possible to stress the sample by bending or torsion individually or in combination. Real bending stress of the sample from Fig. 2 is schematically displayed as follows (Fig. 3):

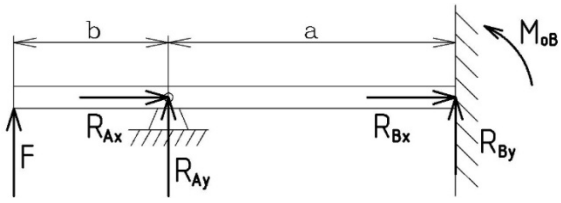

Fig. 3. Forces acting on the sample under bending stress

The suitability of the sample geometry was verified according to the distribution of bending moment. It means that the maximum bending stress has to be at the site of stress concentrator e.g. in the middle of the sample. The length *s* results from Fig. 4 as follows:

$$s = \frac{d_o}{2} + R \tag{1}$$

$$l = \sqrt{R^2 - \left(s - \frac{D}{2}\right)^2} \tag{2}$$

$$\frac{d_x}{2} = s - \sqrt{R^2 - \left(a_1 + l - x_2\right)^2} \tag{3}$$

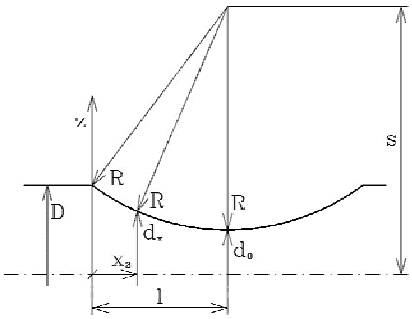

Fig. 4. The sample neck geometry dependent on variable x

The moment of inertia in the part a_1 and a_3 (see Fig. 5) will be as follows:

$$J_y(x_1) = J_y(x_3) = \frac{\pi \cdot D^4}{64} \tag{4}$$

More complicated is the part a_2:

$$J_y(x_2)=\frac{\pi\cdot d_x^4}{64}=\frac{\pi\cdot r_x^4}{4}= \\ =\frac{\pi\cdot\left[s-\sqrt{R^2-(a_1+l-x_2)^2}\right]^4}{4} \tag{5}$$

When boundary conditions are as follows:

$$0\le x_1\le a_1 \\ M_o(x_1)=M_{oF}+R_A\cdot x_1 \tag{6}$$

$$a_1\le x_2\le a_2 \\ M_o(x_2)=M_{oF}+R_A\cdot x_2 \tag{7}$$

$$a_2\le x_3\le a_3 \\ M_o(x_3)=M_{oF}+R_A\cdot x_3 \tag{8}$$

according to Castiglian $\frac{\partial U}{\partial R}=0$.

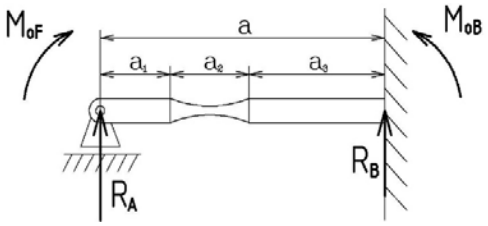

Fig.5. Simplified diagram of the load

Statically indeterminate value (R_A in the Fig. 5) causes minimum internal energy i.e. zero. The internal energy will be as follows:

$$U=\int_{(l)}\frac{M_o{}^2dx}{2E\cdot J_y} \tag{9}$$

$$0=\int_0^{a_1}\frac{M(x_1)}{E\cdot J_y(x_1)}\cdot\frac{\partial M(x_1)}{\partial R_A}dx_1+\int_{a_1}^{a_2}\frac{M(x_2)}{E.J_y(x_2)}\cdot\frac{\partial M(x_2)}{\partial R_A}dx_2+ \\ +\int_{a_2}^{a_3}\frac{M(x_3)}{E.J_y(x_3)}\cdot\frac{\partial M(x_3)}{\partial R_A}dx_3,$$

$$0=\int_0^{a_1}\frac{M_{oF}+R_A.x_1}{E.J_y(x_1)}.x_1dx_1+\int_{a_1}^{a_2}\frac{M_{oF}+R_A.x_2}{E.J_y(x_2)}x_2dx_2+ \\ +\int_0^{a_3}\frac{M_{oF}+R_A.x_3}{E.J_y(x_3)}.x_3dx_3,$$

$$0=\int_0^{a_1}\frac{M_{oF}.x_1}{E.J_y(x_1)}dx_1+\int_{a_1}^{a_2}\frac{M_{oF}.x_2}{E.J_y(x_2)}dx_2+\int_{a_2}^{a_3}\frac{M_{oF}.x_3}{E.J_y(x_3)}dx_3+$$

$$+\int_0^{a_1}\frac{R_A.x_1^2}{E.J_y(x_1)}dx_1+\int_{a_1}^{a_2}\frac{R_A.x_2^2}{E.J_y(x_2)}dx_2+\int_{a_2}^{a_3}\frac{R_A.x_3^2}{E.J_y(x_3)}dx_3$$

R_A expressed from above equation is:

$$R_A=\frac{\int_0^{a_1}\frac{64M_{oF}.x_1}{E.\pi.D^4}dx_1+\int_{a_1}^{a_2}\frac{4M_{oF}.x_2}{E.\pi.\left[s-\sqrt{R^2-(a_1+l+x_2)^2}\right]^4}dx_2+\int_{a_2}^{a_3}\frac{64M_{oF}.x_3}{E.\pi.D^4}dx_3}{\int_0^{a_1}\frac{64x_1^2}{E.\pi.D^4}dx_1+\int_{a_1}^{a_2}\frac{4x_2^2}{E.\pi.\left[s-\sqrt{R^2-(a_1+l+x_2)^2}\right]^4}dx_2+\int_{a_2}^{a_3}\frac{64x_3^2}{E.\pi.D^4}dx_3}$$

$$\sigma(x_1)=\frac{M_o(x_1)}{W_o(x_1)} \tag{10}$$

$$\sigma(x_2)=\frac{M_o(x_2)}{W_o(x_2)} \tag{11}$$

$$\sigma(x_3)=\frac{M_o(x_3)}{W_o(x_3)} \tag{12}$$

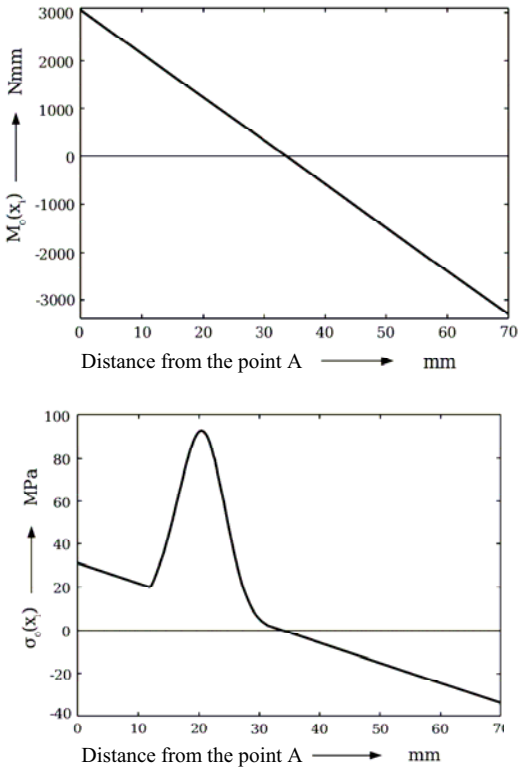

Fig. 6. Lengthwise distribution of the sample bending moment (above) and lengthwise distribution of the normal bending stress (down)

Results of analytical calculation show the necessity to replace the notch from the centre of the sample to the left jaw causing bending stress of the sample. Then the maximum bending stress will be at the point of the stress-raiser. This ensures that fatigue failure can be expected in the place of the notch that is near the left jaw (Fig. 6). After final sample geometry design established by calculation, the technical drawing (Fig. 7) and subsequently a technological process of samples production were made.

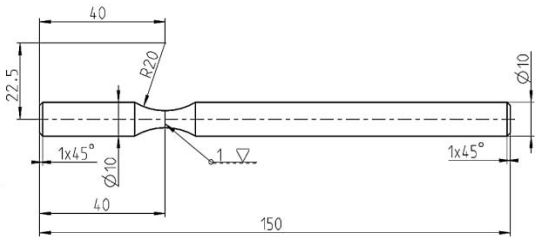

Fig. 7. Valid sample geometry for evaluation of fatigue of weld joints

Since this sample is intended for evaluation of the fatigue of weld joints, it is necessary to locate the weld joint at the stress-raiser site. By this, technological problem occurred that needed to be solved.

4. WELDING TECHNOLOGY SELECTION

There is a great number of welding technologies, therefore making a choice of one of them for sample production is needed. Preferably, we apply the method of welding with non-melting tungsten electrode in an inert gas – TIG [6, 7]. At this welding technology, the arc burns between the non-melting tungsten electrode and the base material in the shielding gas atmosphere of argon. TIG is in the group of arc welding realised at high temperatures causing the associated material to locally melt and form weld pool. Aluminium and its alloys are welded only by alternating current with high voltage ignition or pulse ignition. Our goal was to compare the fatigue life of welded samples with that of samples without weld. Therefore, it is important to achieve the weld joint with high mechanical properties - in particular weld strength. At the start of the fatigue test, the value of residual strength after welding is equal to the static strength of the test sample. During the fatigue test, degradation of residual strength occurs. At certain time, the value of this quantity reaches the maximum possible load value and it causes a malfunction. It is therefore desirable to achieve a weld joint with strength comparable to that of base material, what is however difficult at welding aluminium and its alloys [8, 9]. Weld joint was created by Fronius Magic Wave 2200 welder using the following welding parameters: welding current I_z= 79 A, welding arc voltage U_z was around 18.8 V, the diameter of the tungsten electrode Ød = 2.4 mm, the diameter of the additional material AlSi5 Ø = 2 mm, shielding gas: 99.996% Ar at a flow rate Q = 15 l.min^{-1}.


Fig. 8. Real weld joint

The welding current value was used because of the stable burning arc during welding. A high value of current has not been desirable, because the workpiece is due to its dimensions not allowed to warm up to high temperature because of the melting entire volume of sample metal.

5. WELDING SIMULATION

The main objective of the use of numerical simulations of welding in industry is to determine the deformations of parts and the possibility of errors - based on parameters such as material structure, hardness, residual stress and the total plastic deformation. Furthermore, numerical simulations allow detailed understanding of the whole technological process, since it permits insight on the results of in-process (strain, structure, stress etc.) what the bulk of the experimental measurements do not enable or in very limited extent [10]. The first step at addressing this issue was creating FEM model of weld sample (Fig. 9). For this purpose, computer software called SysWeld belonging to the world's top programs for a complete solution to the problems of weld joints was used.

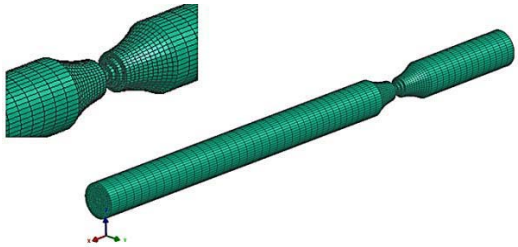
Fig. 9. Creating weld area on the sample model; simulation created in the program SysWeld

Using the same shape of weld surfaces as used for welding practice would lead to acute angles in the elements and thus problem with FEM mesh creation [11-13]. Therefore, weld surface shape was suitably modified. However this, from technological point of view, does not affect weld joint differently than the shape used at welding practice. The only difference would be the creation of complicated weld area on the actual sample. After creating the model, simulation of welding samples was performed (Fig. 10).

The temperature at contact of the electrode with the workpiece, at time t = 0.5 s reached a maximum value of 288 ° C. At this time, yet cold ends of the sample had temperature of 44 ° C. Over the next two seconds, temperature reached the maximum value of 560 ° C at the welding site. The temperature at the free ends was still relatively low 75 ° C. Their heating is indirect and caused by conduction.

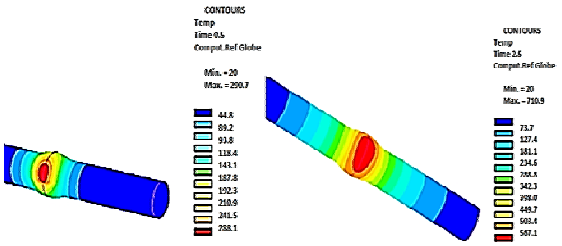

Fig. 10. Temperature gradient at welding at time t = 0.5 s (left) and at time t = 2.5 s (right)

Conduction depends on the coefficient of thermal conductivity λ of the material. The more is increased the amount of alloying elements in the alloy, the more decreases the thermal conductivity of the material [14, 15]. Aluminium itself conducts heat very well, but it is in this case undesirable as structure overheats during welding in the whole volume of the sample. Time of sample welding and simulation of the sample welding was 30 seconds. During this period, the weld joint with a strength of 166 MPa was created, which was proved by tensile test. Temperature distribution immediately after the completion of welding explains Fig. 11. Immediately after welding, the maximum temperature was observed in the weld spot. It reached value of 410 ° C. The lowest temperature was on the longer side of the workpiece to the weld and its value was 105 ° C.

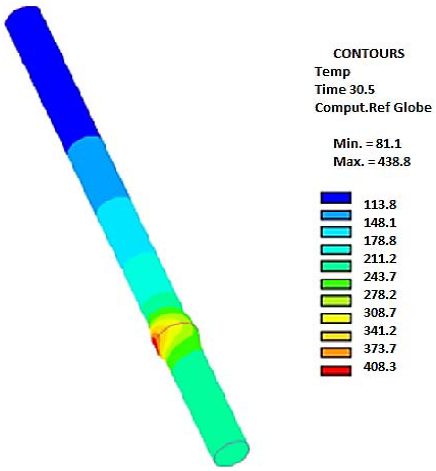

Fig. 11: Temperature distribution at time t = 30.5 s

Temperature distributions were important for assessing the size of the heat affected zone, which took part in measuring the hardness of each area of the weld joint. Next step of the preparation of the sample was its gradual cooling in the air at 20 ° C in order to allow handling of the sample. The time was approximately 1 hour. The result of welding simulation is the FEM model with maximum displacement, caused by the heat at the time t = 30 s and showed in the Fig. 12.

This computational model was used not only for carrying out the analysis of the displacement during welding, but also for inspection of the material phase changes due to the temperature as well as the detection of stresses and strains in real time. In Fig. 13 there is displacement in nodes, shown at time t = 30 s, which is time of the largest displacement observed in the sample during welding. Offset value was 0.306 mm at the weld site, namely at a fusion boundary.

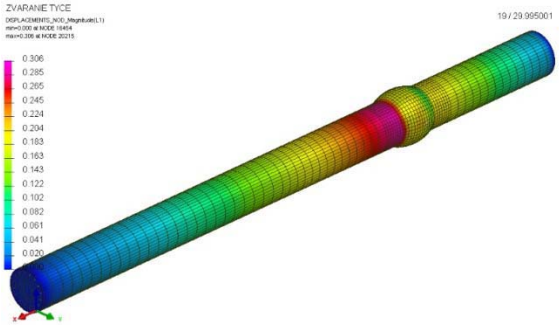

Fig. 12. Maximum total displacements of the sample at time t = 30 s

Under the influence of different temperatures and chemical composition of the base and additional material during welding, phase changing occurred that could therefore remain in the sample volume after cooling.

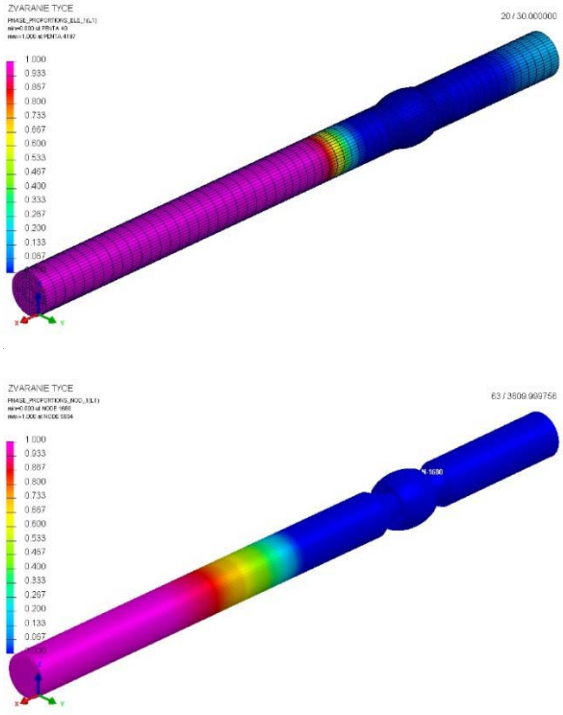

Fig. 13. The percentage of phase 1 (base material) at the end of welding the sample t = 30 s (above), and after cooling at time t = 3600 s (down)

Phase 1 is the base material not affected by temperature during welding (Fig. 13 above - part of the sample with a pink colour). After cooling to 20°C a change in phase 1 was observed. Reason for this is a high temperature of the weld bead after welding, which spread further into material by conduction and thus influenced it by heat (Fig. 13 down). The weld joint is formed by two semi-circular shaped beads. Phase 2 is a representation of the weld metal (Fig. 14 above), and its temperature affected state in the bead no. 1. Simulation for phase 3 is similar (Fig. 14 down), because the bead is formed in the same welding process, using the same additional material and welding parameters as at the first bead was.

After cooling, the percentage of phases 2 and 3 (weld metal) in the sample will be as explained in Fig. 15 above. The last phase of the sample during welding is the heat-affected zone (Fig. 15 down). It is an area that was not melted by the welding heat input, but the thermal field was so huge that a change in the structure occurred.

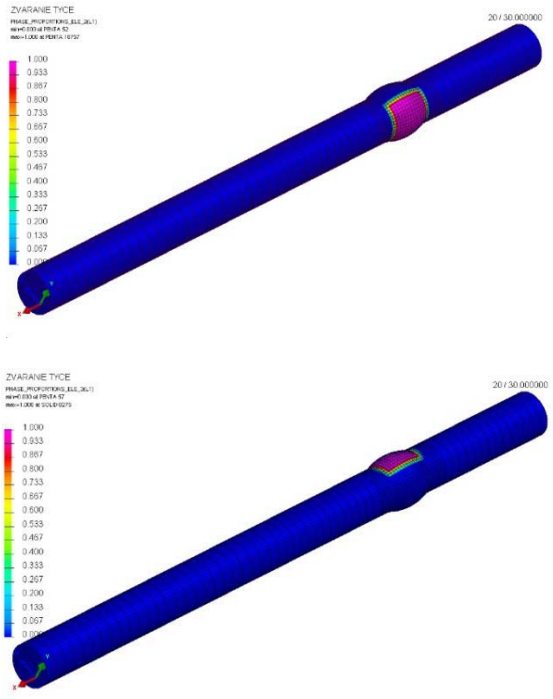

Fig. 14. The percentage of phase 2 (weld metal of the first bead) at the end of welding the sample t = 30 s (above) and phase 3 (weld metal of the second bead) (down)

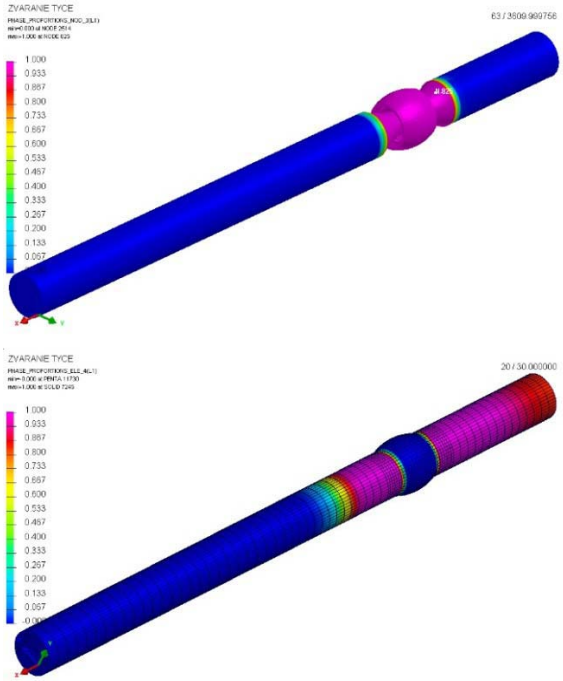

Fig. 15. The percentage of additional material in the sample after cooling (left) and the percentage of the heat affected zone (right)

Conclusion

As shown by the above results, a prerequisite to obtain correct results in simulation program SysWeld is a correct determination of boundary conditions. Therefore, appropriate sample geometry with notch shape and positioning was designed and computationally verified in this paper. With respect to the material used - aluminium alloy, TIG welding technology was opted. Approaching real conditions of the sample after welding was managed using numerical simulations. It was found that proper assessment of the properties of different materials requires an analysis of possible sample loading and application of the simulation program. The next step of addressing this issue will be experimental detection of fatigue characteristics in the diagnostic workplace of fatigue measurement (Fig. 16 above) on designed multiaxial fatigue testing equipment (Fig. 16 down) [13, 16].

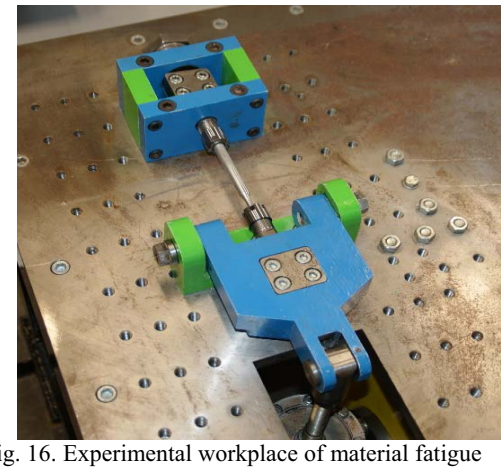

Fig. 16. Experimental workplace of material fatigue measurement (above) and multiaxial testing equipment (down)

REFERENCES

[1] Antoszewski B, Tofil S. The laser welding of iridium-platinum tips to spark plug electrodes. Proceedings of SPIE – The International Society for Optical Engineering. 2016; 10159.
[2] Skrucany T, Gnap J. The effect of the crosswinds on the stability of the moving vehicles. Applied Mechanics and Materials. 2014; 617: 296-301.
[3] Jedlinski L, Caban J, Krzywonos L, Wierzbicki S, Brumercik F. Application of vibration signal in the diagnosis of IC engine valve clearance. Journal of Vibroengineering, 2015; 17(1): 175-187.
[4] Patek M, Sladek A, Mician M. Destructive testing of the weld joints on split sleeve for branch connections repairs. Komunikacie – vedecke listy Zilinskej univerzity, Communications: scientific letters of the University of Žilina. 20154; 17(4): 65-69.
[5] Wanklade RJ, Bajoria K. Numerical optimization of piezolaminated beams under static and dynamic excitations. Journal of Science: Advanced Materials and Devices. 2017; 2: 255-262.
[6] Singh G, Kang AS, Singh K, Singh J. Experimental comparison of friction stir welding process and TIG welding process for 6082-T6 Aluminium alloy. Materials Today: Proceedings 4. 2017; 4(2A): 3590-3600.
[7] Kumar A, Sundarrajan S. Optimization of pulsed TIG welding process parameters on mechanical properties of AA 5456 Aluminum alloy weldments. Materials & Design. 2009;30: 1288–1297.
[8] Eibl M, Sonsino CM, Kaufmann H, Zhang AG. Fatigue assessment of laser welded thin sheet aluminium. International Journal of Fatigue. 2003;25(8): 719-731.
https://doi.org/10.1016/S0142-1123(03)00053-7
[9] Xu YL, Dong ZB, Wei YH, Yang CL. Marangoni convection and weld shape variation in A-TIG welding process. Theoretical and Applied Fracture Mechanics. 2007; 48(2): 178–186.
[10] Alipooramirabad H, Paradowska A, Ghomashchi R, Reid M. Investigating the effects of welding process on residual stresses, microstructure and mechanical properties in HSLA steel welds. Journal of Manufacturing Processes. 2017; 28(1): 70-81.
https://doi.org/10.1016/j.tafmec.2007.05.004
[11] Piekarska W, Rek K. Numerical analysis and experimental research on deformation of flat made of TIG welded 0H18N9 steel. Procedia Engineering. 2017; 177: 182-187.
[12] Wikary T, Radkowski S, Dybala J, Lubikowski K. Modelling of thermoelectric processes in FEM environment based on experimental studies. Springer Proceedings in Mathematics and Statistics. 2016; 181: 395-403.
[13] Kubiak M, Domanski T, Dekýš V, Sapietová A. Measurement of strain during tension test of welded joint using multi-camera 3D correlation. Procedia Engineering. 2017; 177: 107-113.
[14] Sapieta M, Dekýš V, Sapietova A. Thermal-stress analysis of beam loaded by 3 point bending. Procedia Engineering. 2016: 136: 216-219.
[15] Sapieta M, Dekys V, Sapietova A. Thermal stress analysis of beam loaded by 3 point bending. Procedia engineering. 2016; 136: 216-219.
[16] Gerlici J, Lack T, Harusinec J. Development of test stand prototype for rail vehicles brake components testing. Komunikacie – vedecke listy Zilinskej univerzity, Communications: scientific letters of the University of Žilina. 2014; 16: 3A: 27-32.

Acknowledgement

This contribution is the result of the project implementation: "Modern methods of teaching of control and diagnostic systems of engine vehicles", ITMS code 26110230107, supported by the Operational Programme Education and VEGA 1/0927/15 "Research of the use of alternative fuels and hybrid drives on traction vehicles with aim to reduce fuel consumption and air pollutants production".

Received 2017-08-08
Accepted 2017-10-06
Available online 2017-11-06

Ing. **Miroslav BLATNICKY,** PhD. is the university teacher at the Department of Transport and Handling Machines of Faculty of Mechanical Engineering of University of Ņilina. His scientific fields of interest relate to the strength calculations and simulation of transport and handling machines.

doc. ing. **Dalibor BARTA,** PhD. is the university professor at the Department of Transport and Handling Machines of Faculty of Mechanical Engineering of University of Zilina. His scientific fields of interest relate to the simulation and design of non-convention drives of vehicles and using of alternative drives based on the real operating conditions.

Ing. **Jan DIZO,** PhD. is the university teacher at the Department of Transport and Handling Machines of Faculty of Mechanical Engineering of University of Zilina. His scientific fields of interest relate to the simulations vehicle of dynamics.

Paweł DROZDZIEL, Ph.D., D. Sc. (Eng.), Assoc. Prof. the Institute of Transport, Combustion Engines and Ecology, Vice-Rector of Lublin University of Technology.